Hybrid analytic-numeric method for light through a bounded planar dielectric structure

J. B. Nicolau* and E. van Groesen

Department of Applied Mathematics, MESA$^+$ Research Institute,
University of Twente, The Netherlands

We present a hybrid analytic-numeric method to calculate the transmission and reflection of light that is fluxed into a bounded complicated optical structure surrounded by air. The solution is obtained by numerically calculations inside a square containing the structure and by analytical calculations outside the square. For solving the 2D Helmholtz equation we formulate Transparent-Influx Boundary Conditions (TIBC's) on the boundaries of the square; these are incorporated into a variational formulation of the Helmholtz equation to obtain a FEM-implementation for the interior calculations.

Keywords: Transparent-Influx Boundary Conditions, Dirichlet-to-Neumann operator, Helmholtz problems, hybrid analytic-numeric method, Finite Element Method.

1 Introduction

Usually, when numerically computing the solution of optical problems in an unbounded domain, artificial boundaries are introduced to confine the infinite domain to a finite computational window. For reasons of efficiency, this window should be as small as possible. The corresponding boundary conditions must be chosen such that reflectionless propagation of waves through this boundary can be modelled and that arbitrary influx can be prescribed. These boundary conditions are commonly named as *Transparent Boundary Conditions* or *Nonreflecting Boundary Conditions*, although a few other names are also used [1].

In the past two decades, much research has been done to develop TIBC's which can be divided into two sets: nonlocal and local TIBC's. Concerning nonlocal TIBC's, the main ingredient is the Dirichlet-to-Neumann operator [2] which is typically exact, whereas local TIBC's are usually approximate. Many local approximate boundary conditions have been proposed such as of Engquist and Majda [3], Bayliss and Turkel [4], Higdon [5], Keller & Givoli [1, 6, 7]. Berenger [8] proposed a novel technique called Perfectly Matched Layers (PMLs) which is widely employed. In this approach an absorbing boundary condition is chosen in which an artificial layer of lossy material is placed around the bounded domain. Such boundary conditions may cause spurious modes into the computational window. Nonlocal DtN operators can prevent these spurious modes and can be incorporated in a method to obtain the solution on the whole plane, as we shall show.

We present a hybrid analytic-numeric method for computing solutions of the Helmholtz problem with rectangular shape of the artificial boundary. Our approach uses plane wave decomposition to express the DtN operators. The boundary conditions for the confined problem are incorporated into a variational formulation of the Helmholtz problem and are then implemented using standard FEM discretization. The properties of those boundary conditions depend only on the behavior of the solution in the exterior domain, such that the problem inside the computational window can be arbitrary complex. These boundary conditions guarantee reflectionless propagation of waves through the boundary, and contain no adjustable parameters or artificial adjustment of the physical problem. We emphasize that our boundary conditions are not only transparent but also permit computation of the solutions in the exterior using the boundary values of the numerically calculated interior solution. A method for 2D Helmholtz problem on a rectangular domain is also presented in reference [9], the method is based on a rigorous mode expansion technique using eigenmodes of waveguides.

* *Jaqueline B. Nicolau, Department of Applied Mathematics, University of Twente, P.O. Box 217, 7500 AE Enschede, The Netherlands. E-mail: j.b.nicolau@math.utwente.nl*

The outline of this paper is as follows. In Section 2, the general framework for solving the Helmholtz equation for planar optical problems is presented. Section 3 is devoted to a description of Dirichlet-to-Neumann operators and its implementation in case of a square domain. In Section 4, the FEM implementation of the nonlocal boundary conditions is detailed and in Section 5 numerical results are shown to illustrate the performance of the method. In Section 6, we show results of the hybrid character of our method: analytic computations of the exterior solution. Section 7 outlines the extension of the method to the case of TM-polarization of the field. Our conclusions and remarks are discussed in Section 8.

2 General approach

Small devices manipulate light that is often fluxed into the device through air or through waveguides that extend to "infinity". Since light is an electromagnetic wave, its behavior is described by Maxwell's equations whenever it propagates in free space or interacts with matter. Analytic solutions for most optical problems are not available and numerical methods are required to solve them.

On the plane, when restricting to TE-polarization, the propagation of time-harmonic light is described by the scalar Helmholtz Equation (HE) for the principal component E of the electric field perpendicular to the plane,

$$\Delta E + k^2 E = 0,$$

where $k(x,z) = k_0 n(x,z)$, with k_0 the free-space wavenumber, $n(x,z)$ is the refractive index of the media characterizing the geometry of the device, and $k_0 = \frac{2\pi}{\lambda}$, λ is the vacuum wavelength.

We suppose that there is a bounded planar domain Ω with dielectric properties determined by $k_\Omega^2(x,z)$ in a uniform exterior Ω^c with k_0^2. Given a certain influx field E^{in} from the uniform medium, we will determine the solution of the Helmholtz equation both within the dielectric domain as well as in the exterior.

To perform numerical calculations inside Ω, the problem is that the boundary should be able to transfer prescribed influx and be transparent for unknown outflux (including radiation). The approach is to define transparent-influx boundary conditions on $\partial\Omega$ such that the interior problem

$$\Delta E + k_\Omega^2 E = 0 \text{ in } \Omega, \text{ \& TIBC's on } \partial\Omega$$

is a formulation that is suitable for numerical calculations, for instance for calculations based on Finite Element Methods. The TIBC's formulate the influx through the boundary: $E^{in}|_{\partial\Omega}$, and are transparent for outgoing fields.

The numerical solution E_Ω will provide Dirichlet data on $\partial\Omega$; the part $E_\Omega|_{\partial\Omega} - E^{in}|_{\partial\Omega}$ will determine the outgoing field E^{out} so that the total exterior solution is given by

$$E^{ext} = E^{in} + E^{out} \text{ in } \Omega^c.$$

By construction of the TIBC's, the interface conditions on $\partial\Omega$ for solutions E_Ω in the interior and E^{ext} in the exterior are satisfied to guarantee a solution on the plane.

Analytic expressions for TIBC's can be found if DtN operators for the exterior uniform domain can be found. Here we will derive these operators for the case that Ω is a rectangle, based on explicit expressions for exterior solutions using plane wave analysis. Another case in which these operators can be calculated is for the uniform exterior of circular disk, and the general idea above can be applied.

Summarizing the method, for given influx in exterior E^{in}, we formulate TIBC's on $\partial\Omega$, which will include influx information $E^{in}|_{\partial\Omega}$, then we calculate numerically the solution E_Ω in Ω with TIBC's on $\partial\Omega$, from which we can determine the boundary value and calculate analytically the exterior outgoing field from $E_\Omega|_{\partial\Omega} - E^{in}|_{\partial\Omega}$. The interior solution E_Ω and the exterior solution $E^{ext} = E^{in} + E^{out}$ in Ω^c satisfy the correct continuity conditions on $\partial\Omega$ and hence form a solution on the whole plane.

3 Transparent-influx boundary conditions

We now consider the case of a rectangular domain $\Omega = [0, L_x] \times [0, L_z]$ and we assume that the influx is only through the western boundary (see Fig. 1).

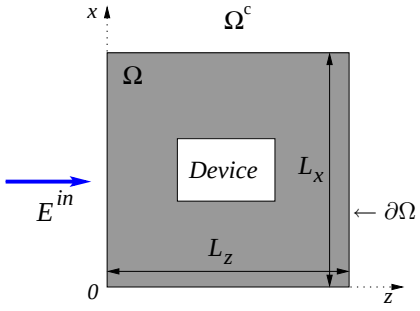

Figure 1: Geometry of the problem. The computational window Ω is a rectangular domain of length L_z and width L_x. Light is fluxed through the western boundary. The Computational window is dressed up with TIBC at the western boundary and transparent for outflux at the remaining ones. The interior domain can be arbitrary complex but the exterior domain is assumed to be uniform to be able to compute the DtN operators.

3.1 TIBC's for calculations in the interior domain

Given an influx field E^{in}, and an a priori unknown outgoing field E^{out}, which will depend on the outgoing light from inside the domain Ω, we now want to formulate boundary conditions on $\partial\Omega$ so that the numerically computed solution in the interior can be extended to a solution on the whole plane. This requires continuity of the field and the normal derivative

$$\partial_n E_\Omega = \partial_n(E^{in} + E^{out}) = \partial_n(E^{in}) + \partial_n(E^{out}) \text{ on } \partial\Omega. \tag{1}$$

Next, we introduce the *Dirichlet-to-Neumann operators*. For given Dirichlet data g at the boundary $\partial\Omega$, two operators are defined as the map to the Neumann data

$$\begin{aligned} D^+(g) &= \partial_n E|_{\partial\Omega} \quad \text{with } E \text{ outgoing solution of the HE with } E|_{\partial\Omega} = g \\ D^-(g) &= \partial_n E|_{\partial\Omega} \quad \text{with } E \text{ incoming solution of the HE with } E|_{\partial\Omega} = g. \end{aligned}$$

Here 'outgoing', respectively 'incoming', refers to the condition to be satisfied at infinity: the outgoing, respectively incoming Sommerfeld radiation condition (SRC), see [10] for details. We will consider for uniqueness of defining 'incoming' and 'outgoing' waves, time-harmonic dependence $e^{-i\omega t}$ of the fields. In here, $\omega = kc$ is the frequency, k is the wavenumber and c is the speed of light.

Thus, in equation (1), $\partial_n(E^{in}) = D^-(E^{in}|_{\partial\Omega})$ is known, but $\partial_n(E^{out}) = D^+(E^{out}|_{\partial\Omega})$ is unknown since E^{out} is unknown. Using continuity on $\partial\Omega$, $E_\Omega = E^{out} + E^{in}$ it follows $E^{out} = E_\Omega - E^{in}$ at $\partial\Omega$ and hence

$$\partial_n(E^{out}) = \partial_n(E_\Omega - E^{in}) = D^+(E_\Omega|_{\partial\Omega}) - D^+(E^{in}|_{\partial\Omega})$$

from which we get the general form of the transparent-influx boundary condition:

$$TIBC: \ \partial_n E_\Omega - D^+(E_\Omega|_{\partial\Omega}) = D^-(E^{in}|_{\partial\Omega}) - D^+(E^{in}|_{\partial\Omega}).$$

For the specific case under consideration, the square with influx through the western side, and using obvious notation for north, east, south and west quantities, we find as boundary conditions:

$$\begin{aligned} &\partial_n E_\Omega - D_W^+(E_\Omega|_{\partial\Omega}) = D^-(f) - D^+(f) \ \text{ on } \partial\Omega_W \text{ with } f = E^{in}|_{\partial\Omega}, \\ &\partial_n E_\Omega - D_\gamma^+(E_\Omega|_{\partial\Omega}) = 0 \ \text{ on } \partial\Omega_\gamma \ \text{ for } \gamma = N,\ E,\ S \end{aligned}$$

representing the transparent-influx boundary condition at $\partial\Omega_W$ and transparent outflux conditions at $\partial\Omega_W = \partial\Omega_N \cup \partial\Omega_E \cup \partial\Omega_S$.
Solving the Helmholtz equation in Ω with these boundary conditions produces the solution in the interior E_Ω.

3.2 DtN operators for a half space

In the following we use plane wave decomposition to express the DtN operators and the solutions in a half plane.
Consider for instance the uniform western half plane ($x, z < 0$) and let a Dirichlet boundary value g_W be given at $z = 0$,

$$g_W(x) = \int \widehat{g_W}(k) e^{ikx} dk.$$

Using Fourier representation, the solution of the exterior problem with outgoing SRC is given by

$$E^{out}(x,z) = \int \widehat{g_W}(k) e^{i[kx - \beta(k)z]}\ dk, \text{ for } z < 0$$

where here and in the following we define

$$\begin{aligned} \beta(k) &= \sqrt{k_0^2 - k^2}\ , \quad \text{if } |k| < k_0 \\ &= i\sqrt{k^2 - k_0^2}\ , \text{ if } |k| > k_0. \end{aligned}$$

The solution E^{out} consists of a combination of plane translating waves (for $|k| \le k_0$) and evanescent waves (for $|k| \ge k_0$) that satisfy the outgoing radiation condition. The outgoing solution leads to the Dirichlet-to-Neumann operator D^+:

$$D^+(g_W) = \int i\beta(k) \widehat{g_W}(k) e^{ikx} dk.$$

In the same way the solution of the problem with incoming wave SRC can be written down and leads to the DtN operator D^-

$$D^-(g_W) = -D^+(g_W).$$

3.3 DtN operators for a square

Suppose on the western side we have boundary function g on the interval $[0, L_x]$. We present this function by

$$g(x) = \sum_{m=-\infty}^{\infty} \widehat{g}(m) e^{i[mh_x x]}, \quad \text{with } h_x = \frac{2\pi}{\alpha L_x} \tag{2}$$

with

$$\widehat{g}(m) = \frac{1}{\alpha L_x} \int_0^{L_x} g(x) e^{i[-mh_x x]}\ dx. \tag{3}$$

Notice that the functions $\{e^{i[mh_x x]}\}_{m=-\infty}^{\infty}$ form an orthogonal system of functions on the interval $[0,\ \alpha L_x]$.
Here α is a parameter that is added to prevent some numerical error as follows. Taking $\alpha = 1$ would mean we represent g by a periodic series, with period which is precisely the length of the side. This may cause some problems at the northern and southern boundaries, see Fig. 3 (a).
Therefore we take $\alpha > 1$ which effectively means that we extend the function to be zero outside the basic interval. The periodic continuation from the series representation then will not effect the numerical window which will be supplied with boundary conditions that does not allow any influx at the other sides. If the given function g at the western boundary corresponds to an influx field, this field is given by

$$E^{in}(x,z) = \sum_{m=-\infty}^{\infty} \widehat{g_{in}}(m) e^{i[mh_x x + \beta(mh_x)z]}, \text{ for } z < 0,$$

which leads to the DtN operators at the western boundary

$$D_W^-(E^{in}|_{\partial\Omega}) = -\sum_{m=-\infty}^{\infty} i\beta(mh_x) \widehat{g_{in}}(m) e^{i[mh_x x]}\ . \text{ Similarly, } D_W^+ = -D_W^-.$$

The outgoing fields at the boundaries can be found in a similar manner.

4 Numerical implementation

A numerical implementation of the method above relies on a numerical discretization scheme inside the domain Ω, and the TIBC's. To discretize the interior domain Ω, we derive the algebraic FE system from the variational formulation (see [11]) of the Helmholtz equation:

$$\mathcal{L}(V,E) := \underbrace{\iint_{\Omega} \nabla V \cdot \nabla E_{\Omega} - k_{\Omega}^2 V E_{\Omega} \,\mathrm{d}s}_{Interior} - \underbrace{\int_{\partial\Omega} V \partial_n E^{ext} \,\mathrm{d}l}_{Boundary} = 0 \ , \ \forall V \in H^1(\Omega)$$

with

$$\int_{\partial\Omega} V \partial_n E^{ext} \,\mathrm{d}l = \int_{\partial\Omega} V\{D^+(E_{\Omega}|_{\partial\Omega}) + D^-(E^{in}|_{\partial\Omega}) - D^+(E^{in}|_{\partial\Omega})\} \,\mathrm{d}l. \tag{4}$$

The first part of the bilinear functional $\mathcal{L}$ contains information about the interior domain. The interior HE problem is coupled via boundary conditions to the exterior problem, that is represented by the boundary integral (4).

4.1 Numerical FEM calculations with TIBC's

The variational formulation of the Helmholtz equation is feasible to derive numerical discretizations consistently by approximating E_{Ω} as an expansion of chosen basis functions. More precisely, if we take the simplest piecewise linear elements, we seek the solution as a linear combination of "tent" basis functions $\{\phi_j(x,z)\}_{j=1}^N$:

$$E_{\Omega}(x,z) \cong \sum_{j=1}^{N} \tilde{E}_j \phi_j(x,z).$$

The basis functions ϕ_j are defined by piecewise linear interpolation between the nodal values $\phi_j(x_i,z_i)$,

$$\phi_j(x_i,z_i) = \delta_{j,i}, \ \text{with} \ \ j,i = 1,\ldots,N,$$

with $\delta_{j,i}$ the Kronecker delta and N the number of nodal points.

If we do not take the boundary conditions into account, we end up with a finite element scheme $S\tilde{E} + M\tilde{E} = 0$, where $S = [S_{ji}]$, $M = [M_{ji}]$ are called the stiffness and mass matrices and its entries are evaluated as follows

$$S_{ji} = \int_{\Omega} \nabla\phi_j \nabla\phi_i \,\mathrm{d}s \ \ \text{and} \ \ M_{ji} = -\int_{\Omega} k_{\Omega}^2 \phi_j \phi_i \,\mathrm{d}s.$$

4.2 FEM-implementation of the DtN operators

We next show how the DtN operators can be implemented in a FEM method. In the previous Section we have discussed a technique to solve the Helmholtz equation with TIBC's, in which explicit expressions for DtN operators were derived. In there, we basically considered a Fourier series representation of the boundary functions as in Eqs. (2) and (3) leading to the DtN operator

$$D_W^+(g) = \sum_{m=-\mathcal{M}}^{\mathcal{M}} i\beta(mh_x)\widehat{g}(m)e^{i[mh_x x]},$$

where the range of $m \in [-\mathcal{M},\ \mathcal{M}]$ is taken to be finite for numerical purposes.
In order to evaluate the boundary integral associated to the west side, we take a test function $V = \sum_{p=1}^N v_p\phi_p$ and observe that the function $g(x)$ can be approximate as $g(x) \cong \sum_{q=1}^N g_q\phi_q(x,0)$. In doing so, the discrete version D_W of the DtN operator D_W^+ takes the form:

$$\int_0^{L_x} V D_W^+(g) \,\mathrm{d}l \ \ \cong \ \ \frac{1}{\alpha L_x} \sum_{p,q}^{N} v_p g_q \Big(\sum_{m=-\mathcal{M}}^{\mathcal{M}} i\beta(mh_x)\widehat{\tau}_{qm}\tau_{pm} \Big) \tag{5}$$

with $\widehat{\tau}_{qm} = \int_0^{L_x} \phi_q(x,0)e^{i[-mh_x x]} \,\mathrm{d}x$ and $\tau_{pm} = \int_0^{L_x} \phi_p(x,0)e^{i[mh_x x]} \,\mathrm{d}x$.

We can apply this procedure to obtain the discrete versions of the DtN operators in the east (D_E), north (D_N) and south (D_S) boundaries, resulting into the full algebraic problem,

$$(S + M + (D_W + D_E + D_S + D_N))\tilde{E} + \vec{F} = 0,$$

with $\vec{F}$ the discrete version of the incoming field $D^-(E^{in}|_{\partial\Omega}) - D^+(E^{in}|_{\partial\Omega})$.
The boundary operator (5) is nonlocal in the sense that it involves an integral operator coupling all points at the boundary. Solving the new system yields some computational effort, however it guarantees transparency, and is easily incorporated in a finite element approach as we have shown.

5 Numerical results

In this Section we show results of the scheme we have derived above. We have implemented these boundary conditions and our numerics were carried out in MATLAB. Simple elements (triangles and rectangles) were used to triangulate the domain. The discretization of the DtN operator results in dense sub-matrices being introduced into otherwise sparse linear systems. The full linear system resulting from the discretization is solved by a direct method (LU decomposition). For accurate performance of our method it is crucial to compute boundary integrals coefficients accurately. The coefficients τ_{qm} and $\widehat{\tau}_{qm}$ in equation (5) were evaluated exactly. However, Fourier coefficients for the given influx were computed using Gauss-Legendre quadrature to approximate them. We have noticed that the optimal choice of the number of harmonic modes is related to the number of nodes used in the discretization. For a square computational window, the best choice is when the number of harmonic modes coincide with the number of nodes.

There is one parameter that has to be chosen in the calculations, namely the factor α (see Eqs. (2) and (3)). Based on our numerical experiments, we found that the value of $\alpha > 1$ can be taken arbitrary as it hardly effects the FEM solution. Simulations in this paper were done taking $\alpha = 2$.

To test the efficiency and accuracy of our method, we show several case studies including comparisons of our computations of Gaussian beams propagating over homogeneous domain with analytic solutions.

5.1 Computing the solution in the interior

Typically, a Gaussian beam $f = e^{-(x-x_a)^2/w^2} e^{ik(\sin\theta x)}$ centered at x_a is launched, which propagates at an angle θ with respect to the z-direction. We choose w to be such that the given influx f is confined in the boundary of the computational window.

We calculate the propagation of such Gaussian beams in a homogeneous medium (air), covered by a computational window of $[0, 10]\ \mu m \times [0, 10]\ \mu m$ surrounded by TBC's. All calculations are meant for a vacuum wavelength of $\lambda = 1\ \mu m$. We have used 200×200 grid points.

Fig. 2 shows the results of various simulations for incident wave parameters as summarized in Table 1. In here θ, w and x_a are the angle, width and waist position of the Gaussian beam, respectively. The subscripts W, E, S and N correspond to Gaussian beams that are fluxed into the domain through the west, east, south and north sides, respectively. We designed TBC's on all sides of the computational window. From Fig. 2 (a)$-$(b), it is seen that the TBC is able to transfer the given influx, and the outgoing one passes the artificial boundary without any noticeable reflection. According to Figs 2 (c)$-$(f), Gaussian beams can be launched through southern (and/or northern) boundary or simultaneously through all four boundaries, as well. Therefore, these boundary conditions are able to transfer prescribed influx and are transparent for unknown outflux.

Since our domain is a square (non-smooth boundary), corner points can give rise to spurious reflections into the domain. To show the effect of the introduction of the parameter α, a centered Gaussian beam of width 1 μm is launched from the western side under a tilt angle of 26.57^0 and should leave the window via northern and eastern boundaries passing through the north-east corner point. Simulations show that our method ($\alpha = 2$) provides a good approximation to the physical solution in the corner region, which suppresses reflections arising from the corner quite efficiently (see Fig. 3 (b)). Much better than when $\alpha = 1$ as shown in Fig. 3 (a), where serious reflections are generated from the corner point.

Table 1: Parameters of the incident beams for Fig. 2.

Plot	θ_W	w_W	x_W	θ_E	w_E	x_E	θ_S	w_S	x_S	θ_N	w_N	x_N
(a)	0^0	2	5	–	–	–	–	–	–	–	–	–
(b)	45^0	2	5	–	–	–	–	–	–	–	–	–
(c)	–	–	–	–	–	–	0^0	0.35	5	–	–	–
(d)	45^0	2	3	45^0	2	3	–	–	–	–	–	–
(e)	10^0	2	5	10^0	2	5	10^0	2	5	10^0	2	5
(f)	45^0	2	5	-45^0	2	5	–	–	–	–	–	–

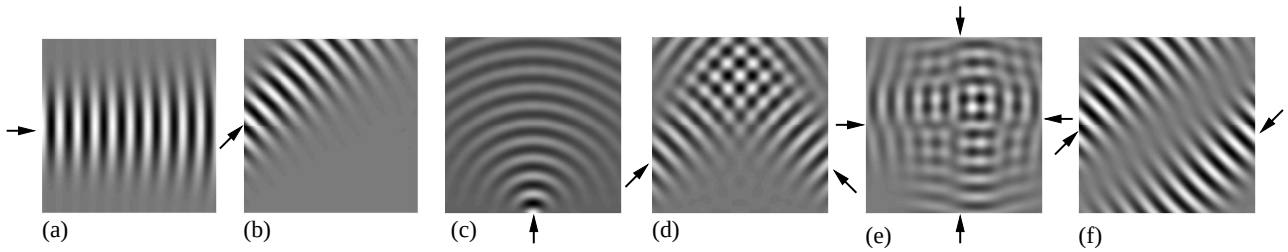

Figure 2: Propagation of Gaussian beams in free space. The plots show snapshots of the electric field profile as a result of FEM calculations with TIBC on the boundary of the computational window as shown.

Figure 3 (d) shows a drawback of the presented numerical method for a plane wave launched through the western boundary. Taking $\alpha > 1$, i.e. introducing a jump at the corner points by extending the influx to vanish outside the basic interval, introduces an undesired diffraction, that is visible in the computational window. For $\alpha = 1$, in Fig. 3 (c) no such effect is noticed, as can be expected.

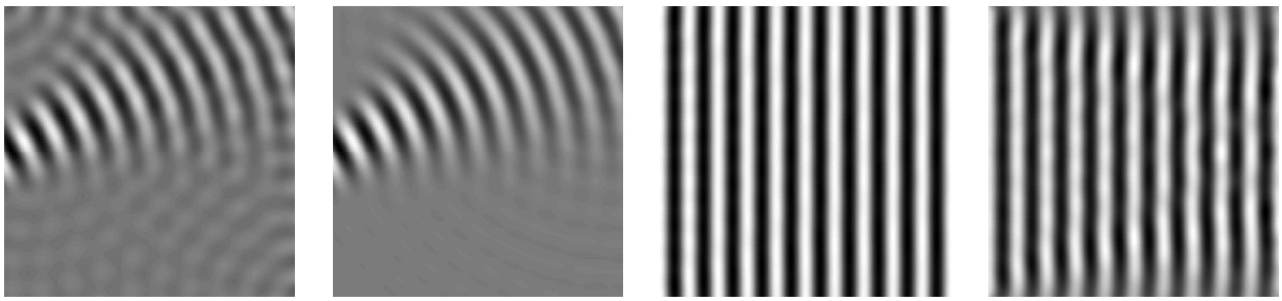

Figure 3: A centered Gaussian beam of width $w = 1\ \mu m$ is launched from the western side towards the north-east corner point. Real part of the fields are shown in case of (a) $\alpha = 1$ and (b) $\alpha = 2$. For a plane wave influxed from the western boundary, the real part of the fields are shown in (c) for $\alpha = 1$ and in (d) for $\alpha = 2$.

Error analysis: to compare the analytic and numeric solution, we recall that an analytical expression for 2D Gaussian beam propagating in homogeneous media is available [12, 13] and is given by

$$
\begin{aligned}
E_G(x,z) &= \sqrt{\frac{w}{W(z)}} e^{-\frac{x^2}{W(z)^2}} e^{i[k(z+\frac{x^2}{2R(z)})-\frac{1}{2}\arctan(\frac{z}{z_r})]}, \quad \text{with} \\
z_r &= \frac{w^2\pi}{\lambda} \text{ the Rayleigh length,} \\
R(z) &= z + \frac{z_r^2}{z} \text{ the radius of curvature of the wave front, and} \\
W(z) &= w\sqrt{1+(\frac{z}{z_r})^2} \text{ the corresponding beam width.}
\end{aligned}
$$

Let us consider the centered Gaussian beam of width 2 μm launched horizontally from the western boundary as in Fig. 2 (a). Using the analytical expression of the 2D Gaussian beam as the exact solution, the following expressions were used for the errors between the computed E_Ω and the analytic solution E_G:

$$L_2 = \frac{(\int |E_\Omega - E_G|^2 \, \mathrm{d}\Omega)^{1/2}}{(\int |E_G|^2 \, \mathrm{d}\Omega)^{1/2}} \text{ and } L_{max} = \frac{\max |E_\Omega - E_G|}{\max |E_G|}.$$

In Fig 4, the comparison between analytic and numeric solution is shown, and the normwise relative error is

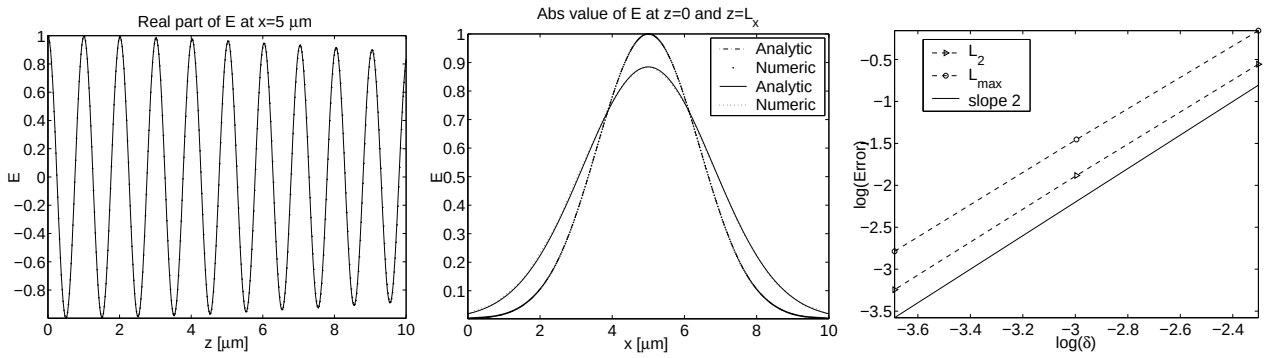

Figure 4: For a Gaussian beam propagating in free space. The first plot is a comparison between numeric and analytic solution at the position $x = 5$ μm, and the second plot at the positions $z = 0,\ 10$ μm. In the third plot, the L_2 and L_{max} errors are shown as function of the stepsize δ.

given as function of the mesh size. The error of the numerical solution shows second order accuracy, as can be expected for the first order elements that are used.

Next, we consider two configurations with inhomogeneous material properties. First, we insert a vertically dielectric rectangular obstacle, with a thickness of 1 μm and a refractive index $n_d = 3.25$. A centered Gaussian beam of width 1.4 μm is launched horizontally, from the western boundary. We have computed the real and absolute value of the field distribution which are shown in Fig. 5 (a)−(b). We have chosen these parameters such that diffraction and refraction occur. In the second configuration, Fig. 5 (c)−(d), an incoming beam of width 1.4 μm and angle 10^0 is placed at $z = 3$ μm (originating from southern boundary). It displays a typical interference pattern of reflected waves.

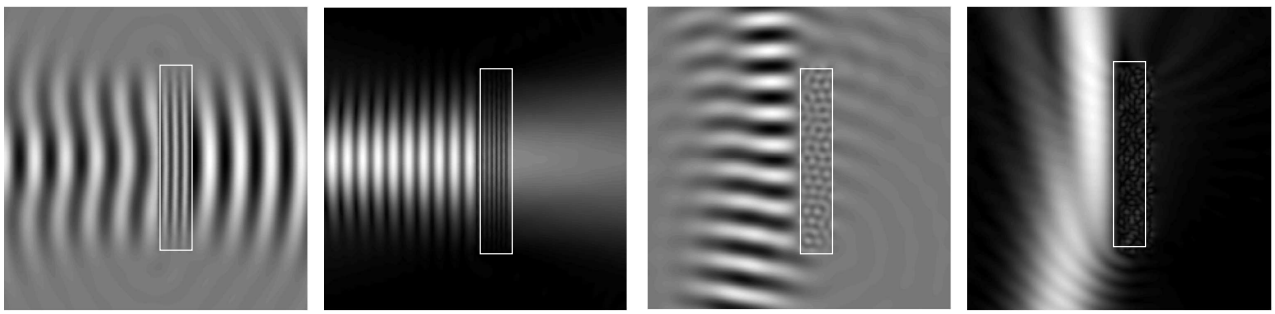

Figure 5: FEM computations are shown of light in a computational window of $[0, 10]$ $\mu m \times [0, 10]$ μm, in which a dielectric rectangle (1 $\mu m \times 6$ μm) with refractive index $n_d = 3.25$ is placed at the center surrounded by air. The light shown in case (a)−(b) is a centered Gaussian beam of width 1.4 μm launched horizontally, and in case (c)−(d) the light is launched from below, tilted at an angle of 10^0. The plots show the real part and absolute value of the field distribution.

6 Analytic representation of exterior solution

Having found the interior solution E_Ω, the Dirichlet data are known at the boundary. Then we can determine the solution analytically in the exterior using the expression for the outgoing solution in half spaces and the boundary values of E_Ω. Denoting these solutions by

$$\begin{array}{llll} E_W^{out} & \text{on} & z<0, & \text{with } E_W^{out}|_{z=0} = E_\Omega|_{z=0} - f \quad \text{with } f = E^{in}|_{z=0} \\ E_E^{out} & \text{on} & z>L_z, & \text{with } E_E^{out}|_{z=L_z} = E_\Omega|_{z=L_z} \\ E_N^{out} & \text{on} & x>L_x, & \text{with } E_N^{out}|_{x=L_x} = E_\Omega|_{x=L_x} \\ E_S^{out} & \text{on} & x<0, & \text{with } E_S^{out}|_{x=0} = E_\Omega|_{x=0} \end{array}$$

we get the total external outgoing solution, in particular by adding the two contributions in the exterior quarter planes (NE, SE, SW, NW), which we denote as E_{NE}^{out}, E_{SE}^{out}, E_{SW}^{out} and E_{NW}^{out}, respectively (see Fig. 6).

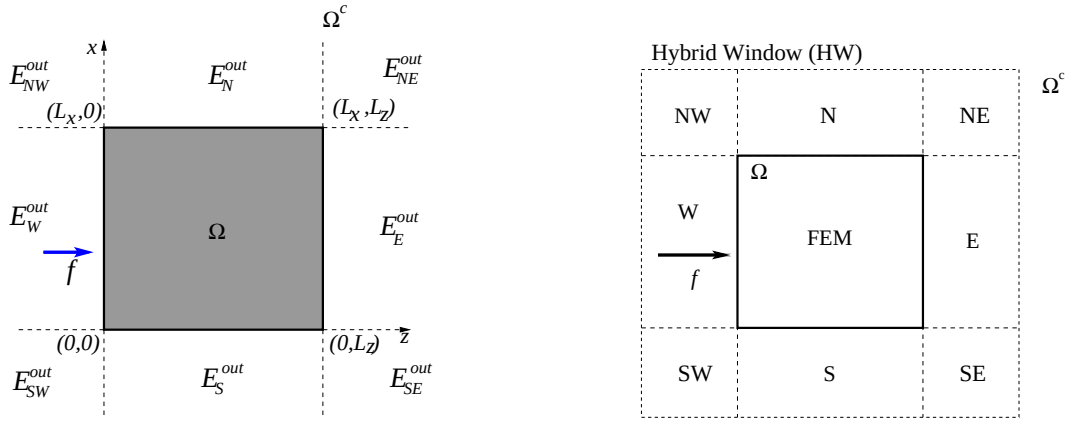

Figure 6: The Hybrid Window (HW) consisting of the interior domain Ω in which we calculate the numerical FEM solution and a region on which the solution is extended in the exterior. Once we have the FEM solution we can obtain the solution in the northern, southern, western and eastern half spaces (N, S, W, E) analytically. The solution in the corner regions is obtained by adding the two contributions in the quarter planes (NW, NE, SE, SW).

The total solution is then obtained by adding the influx field from western half space.
Three numerical results are shown below based on the method presented in this paper. In Figures 7-8 we show results of the absolute value of the calculated solutions on a hybrid window of which the center square 'FEM' is the domain of numerical calculation while the solution is calculated analytically in the other areas. Shown are the case of 7 (a) a horizontally centered Gaussian beam, and (b) an obliquely Gaussian beam with waist position at $x = 3.5\ \mu m$, tilted at an angle of 10^0. In Fig. 8 the interference of two centered Gaussian beams launched through the western and southern boundaries (beam width $w = 2\ \mu m$) is shown. For all the calculations we took $\alpha = 2$, but it should be remarked that the size of the external domain can be arbitrarily large. For instance, in case 7 (a) and 8 the hybrid window is $[-5,\ 15]\ \mu m \times [-5,\ 15]\ \mu m$ and in case 7 (b) the hybrid window is larger $[-20,\ 30]\ \mu m \times [-20,\ 30]\ \mu m$.

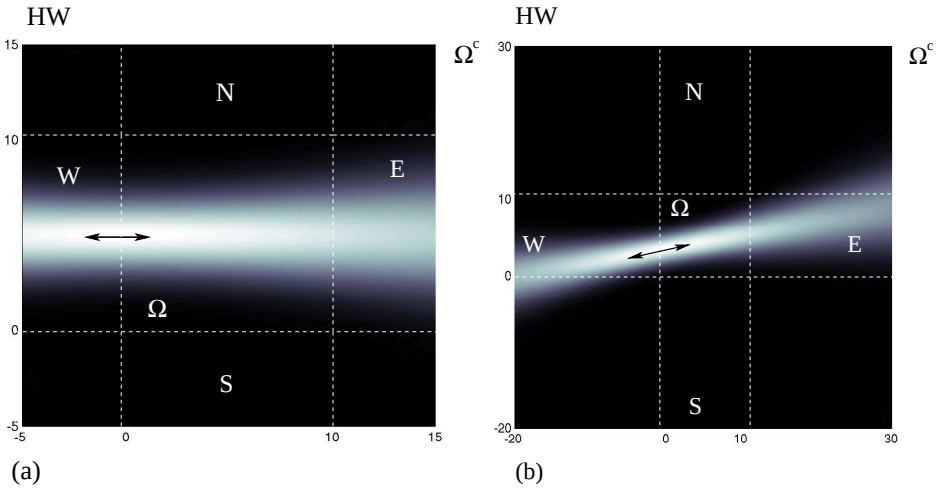

Figure 7: Hybrid Window to calculate Gaussian beams in free space launched through the western boundary of the FE window. The light is shown in case of (a) a horizontally centered Gaussian beam with HW= $[-5,\ 15]\ \mu m \times [-5,\ 15]\ \mu m$ and in case of (b) an obliquely Gaussian beam with HW= $[-20,\ 30]\ \mu m \times [-20,\ 30]\ \mu m$. Absolute value of the field distributions are shown.

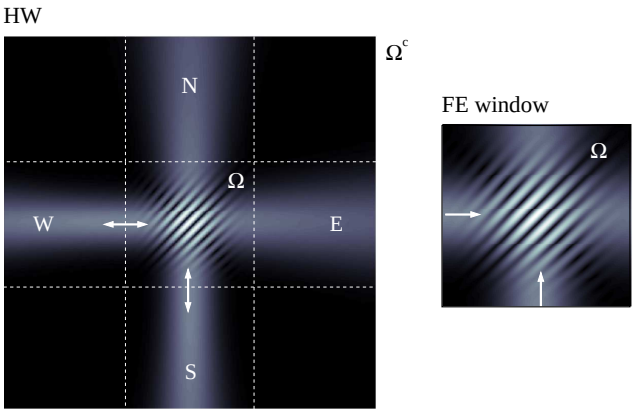

Figure 8: Hybrid Window of $[-10,\ 20]\ \mu m \times [-10,\ 20]\ \mu m$: centered Gaussian beams of $w = 2\ \mu m$ are launched simultaneously through the western and southern boundaries. The absolute value of the numeric solution shows clearly the interference pattern.

7 TM-polarization

For simplicity of exposition, in the description above we restricted to TE-polarization. However the method works just as well for the case of TM-polarization.
The time-harmonic solution with time dependence e^{-iwt} of the Maxwell's equations for TM-polarization is obtained from the Helmholtz equation for the principal component H of the magnetic field parallel to the plane:

$$\nabla \cdot (\frac{1}{n^2}\nabla)H + k_0^2 H = 0,$$

for which the corresponding variational formulation is given by

$$\mathcal{L}(V,H) := \iint_\Omega \frac{1}{n^2}\nabla V \cdot \nabla H - k_0^2 V H \,\mathrm{d}s - \int_{\partial\Omega} \frac{1}{n_0^2} V \partial_n H^{ext} \,\mathrm{d}l \ , \forall V \in H^1(\Omega).$$

For a homogeneous exterior, the treatment of the boundary integral is the same as in case of TE-polarization.

To illustrate the performance, we consider a cube beamsplitter (see Fig. 9), which is a common optical

device to separate an incident light beam into two different polarization beams. The output beam, which is parallel to input beam is the TE-polarized beam, while the orthogonal output beam is the TM-polarized beam.

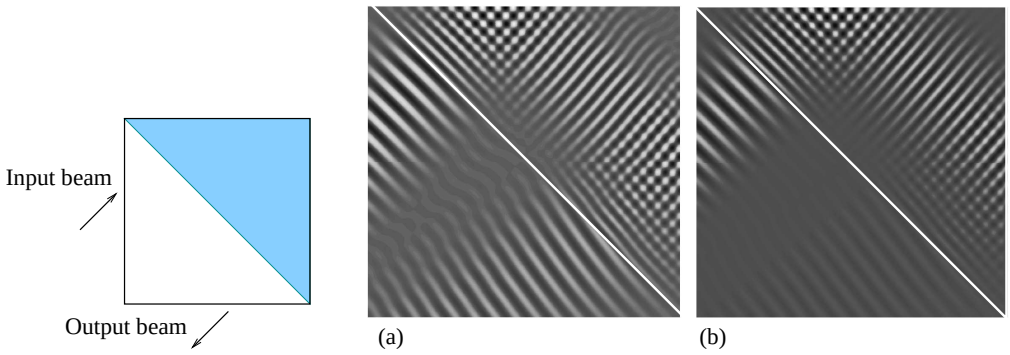

Figure 9: Cube beamsplitter. Real part of the solutions of the HE equation for (a) TE-polarized and (b) TM-polarized incoming field.

The refractive index of the upper-triangular region of the cube is 1.517 (glass) and the wavelength is 0.518 μm. The beam is launched though the western boundary at tilt angle of 45^0 with a beam width of 2 μm. The difference between the two polarizations is very distinct and thus shows the polarization-separating performance of the device.

8 Conclusions

We have developed a framework for constructing nonlocal, well posed boundary conditions for finite element method solutions of Helmholtz equation in 2 D over a rectangular domain. The model is based on the expansion of the DtN operator. We emphasize that the derivation of the boundary conditions depends only on the behavior in the exterior domain, such that the problem inside the computational window can be arbitrary complex. Furthermore, as there is no unphysical reflection at the artificial boundary associated with the computational window, the derived transparent boundary conditions ensure transparency. Regarding the computation efficiency, it should be emphasized that the present formulation takes the advantage of calculating the solution in the exterior allowing one to use smaller computational window.
The TIBC's are formulated as analytical expressions and lead to a well-posed problem; therefore they can be implemented in any numerical program. The TIBC-formulation is not based on a physical perturbation of the problem to be calculated (different from PML). As one consequence we get that for a given exterior influx, the solution in the interior is calculated numerically; the numerical result leads immediately to an analytic expression for the solution of the problem in the exterior. Finally, the TIBC's are formulated here for harmonic problems, TE-modes and TM-modes.

9 Acknowledgments

Support for this work is provided by the Netherlands Organization for Scientific Research (NWO) in computational science program. The authors would like to thank M. Hammer and M. Botchev for fruitful discussions on the subject.

10 References

1. D. Givoli, *J. Comput. Phys.* **94**, 1 (1991).
2. D. Givoli, *Numerical methods for problems in infinite domains* (Elsevier, Amsterdam, 1992).
3. B. Engquist and A. Majda, *Commun. Pure Appl. Math.* **32**, 313 (1979).
4. A. Bayliss and E. Turkel, *Commun. Pure Appl. Math.* **33**, 707 (1980).
5. R. L. Higdon, *Math. Comput.* **49**, 65 (1987).
6. J. B. Keller and D. Givoli, *J. Comp. Phys.* **82**, 172 (1989).

7. D. Givoli, I. Patlashenko and J. Keller, *Comput. Meth. Appl. Mech. Eng.* **143**, 13 (1997).

8. J. P. Bérenger, *J. Comput. Phys.* **114**, 185 (1994).

9. M. Hammer, *Optics Communications* **235** (4-6), 285 (2004).

10. J-C. Nédelec, *Acoustic and Electromagnetics Equations: Integral Representations for Harmonic Problems*, (Springer-Verlag, New York, 2001).

11. E. van Groesen, *Variational modelling for integrated optical devices - Proc. 4th IMACS-symposium on Mathematical Modelling*, TU Vienna, 76 (2003).

12. S. Choudhary and L. B. Felsen, *Proc. IEEE* **62**, 1530 (1974).

13. M. Bornatici and O. Maj, *Plasma Phys. Control. Fusion.* **45**, 707 (2003).